International Journal for Quality Research 20(1) 109–126
ISSN 1800-6450

Henry Francis Annapeh [1]
Victoria Kurushina

Article info:
Received 03.12.2024.
Accepted 10.06.2025.

DOI – 10.24874/IJQR20.01-07

RELIABILITY ASSESSMENT OF CYLINDRICAL OFFSHORE STRUCTURES SUBJECTED TO CROSS-FLOW VORTEX-INDUCED VIBRATIONS IN SHEARED AND PARABOLIC CURRENTS

Abstract: *Cross-flow vortex-induced vibration of offshore structures is a complex, challenging to predict phenomenon with an impact on the structural integrity and lifespan and with the sensitivity to flow conditions. The current study is focused on the cross-flow vibration of a cylindrical structure in the linearly sheared and parabolic flows. The work is performed with the computational fluid dynamics method in 2D for the Reynolds number range of 350-2150, mass ratio of 2 and shear parameter from 0 to 0.05 for the linearly sheared current. The results obtained indicate differences in the width of the upper branch of the lock-in and characteristics of the lower branch related to the sheared flow profile. The study also reports a more stable trend in the growing lift coefficient, mean drag coefficient and frequency ratio in sheared flow, compared to the uniform flow.*

Keywords: *vortex-induced vibrations, sheared flow, parabolic flow, offshore structures, computational fluid dynamics*

1. Introduction

Dynamic response of rigid structures, such as risers and cables, subjected to waves and currents, significantly accelerates the accumulation of the fatigue damage and may disrupt planned offshore operations. Cross-flow response of offshore structures is more significant in the displacement amplitude (Bearman, 1984; Sarpkaya, 2004), and understanding and forecasting the transversal oscillations constitutes the main challenge during the design (Blevins, 1990). Accurate predictions of the cross-flow oscillations is subject of ongoing research efforts in the field of vortex-induced vibrations (VIV), due to sensitivity of the complex phenomenon to the parameter range of the flow and the structure (Williamson & Govardhan, 2004).

Vortex-induced vibration manifests when vortices shed from a bluff object in a fluid flow create alternating forces. This may result in a substantial displacement of the structure, especially as the shedding frequency aligns with the structure's natural frequency (Bearman, 1984), which is often referred to as the lock-in condition (Williamson & Govardhan, 2004; Williamson & Roshko, 1988). The study (Stappenbelt et al., 2007) performs a systematic investigation of the evolution of the cross-flow response for the range of mass ratio from 2.36 to 12.96. The lock-in region observed for the 1 degree-of-freedom (1DOF) structure is deconstructed into the initial branch, upper branch and desynchronization stage, when considered in terms of the structure's displacement. The displacement amplitude is found to increase with reducing mass ratio. In other

[1] Corresponding author: Henry Francis Annapeh
Email: annapeg@tyuiu.ru

experimental work (Blevins & Coughran, 2009), the effect of the structural damping on the displacement amplitude is considered, with a higher amplitude observed for the lower damping ratio.

Effects of the Reynolds number and structural damping on vortex-induced vibrations of elastically-mounted rigid cylinder in three-dimensions were also numerically studied by (Martins & Avila, 2019). Their findings suggested that the desynchronization region widens with higher damping ratios, affecting the overall response of the system. The experiment conducted by (Khalak & Williamson, 1996) found that at very low mass-damping ratios, the response of the cylinder exhibits two distinct lock-ins, with the first lock-in forming around the reduced velocity of 2.5. The work (Khan et al., 2017) emphasized the potential of RANS models to provide reliable predictions of VIV with lower computational costs compared to traditional methods.

Several studies, undertaken for stationary cylinders (Lu et al., 1997; Cheng et al., 2005; Kang, 2006; Cao et al., 2012; Akosile & Sumner, 2003; Bhattacharyya & Dhinakaran, 2008; Lankadasu & Vengadesan, 2008; Annapeh & Kurushina, 2024; Annapeh & Kurushina, 2023), for a single structure or an array of structures, highlighted the importance of the shear parameter's effects on the dynamics of fluid forces, vortex shedding frequency, and flow pattern in planar sheared flow. Vortex-induced vibration of a single circular cylinder in sheared flow was numerically studied by (Zhang et al., 2014) with the stream function-vorticity equation. The shear parameter K values employed in their work were 0, 0.1 and 0.2. Their result revealed that vortices strengthened on one side and weakened on the other side of the structure, together with the shift of front stagnation point. The authors of (Zhao et al., 2012) numerically investigated the 1DOF circular cylinder in the oscillatory flow, using the Petrov–Galerkin finite element method. Simulations were performed for two Keulegan-Carpenter (KC) numbers of 10 and 20 in the reduced velocity range of 1-36. It was found that the dynamic response contains only one frequency component when the reduced velocity is less than 8 for both KC numbers and contains multiple frequency components, as the reduced velocity exceeds 8. The work (Tu et al., 2014) reports the flow-induced vibration of an elastically mounted circular cylinder in a planar sheared flow with 1DOF and 2DOF at the Reynolds number of 150 using the characteristic-based-split (CBS) finite element method. The mass ratio of 2, reduced velocity of 3-12 and shear parameter of 0-0.1 were used in this work. It was demonstrated that, in the 1DOF system, the frequency synchronization region extends with the increase of K. A numerical study by (Singh & Chatterjee, 2014) was focused on the VIV for an isolated circular cylinder in a linear sheared flow at low Reynolds numbers ($70 \leq Re \leq 500$). They revealed that the maximum displacement along the transverse direction does not get affected by the shear parameter introduced at the inlet.

The dynamics of a cylinder in parabolic flow is less explored compared to uniform or linearly sheared flows. Such flows are relevant to many engineering applications, including channel flows and boundary layer interactions. For stationary cylinders, a numerical study was conducted by (Annapeh & Kurushina, 2022; Annapeh & Kurushina, 2023) to analyze the effect of parabolic and linearly sheared flow on a group of subsea structures in proximity of equipment. Although parabolic flow has similarities to sheared flow in terms of velocity gradients, the quadratic velocity profile leads to a more noticeable change in flow forces along the cylinder span. This may result in more intricate wake dynamics and oscillation patterns, an area that has not been fully investigated in existing literature.

The literature review indicates a lack of knowledge on VIV in linearly sheared and parabolic flows for 1DOF elastically mounted circular cylinder, especially at moderate Reynolds numbers of around 300 and at low shear parameter values (K= 0.01, 0.02, 0.03,

0.04 and 0.05). The majority of current research on shear flow is concentrated on high Reynolds numbers, where turbulent wake dynamics has a noticeable impact, and on the high shear parameter K. The current work seeks to compare the effect of linearly sheared and parabolic flow on the maximum displacement, and hydrodynamic coefficients and frequency of an elastically mounted circular cylinder at Reynolds number range of 350-2150. The research is performed for the mass ratio of 2, reduced velocity ranging from 2 to12 and sheared flow parameter K value range of 0.0-0.05.

2. Numerical model

Flow over an elastically mounted circular cylinder subjected to linearly sheared and parabolic flow as shown in Figure 1(a) and 1(b) is investigated numerically. The diameter of the cylinder under investigation has a value of D = 0.01 m. The study is conducted for a constant mass ratio of 2 with the reduced velocity varying in the range of 2-12. The mass ratio of 2 is chosen for this work because engineering structures, vibrating in water, typically have low mass ratios. The computational domain has a total size of 60D x 40D. The cylinder is located at a distance of 20D from the inlet boundary. The width of the domain is 40D with the cylinder located in the middle. The inlet boundary is defined as the velocity-inlet and the outlet is pressure-outlet with a zero-gauge pressure. The top and bottom of the computational domain is defined as symmetry with no-slip condition applied to the surface of the cylinder. The natural frequency of the structure is 1.8 Hz.

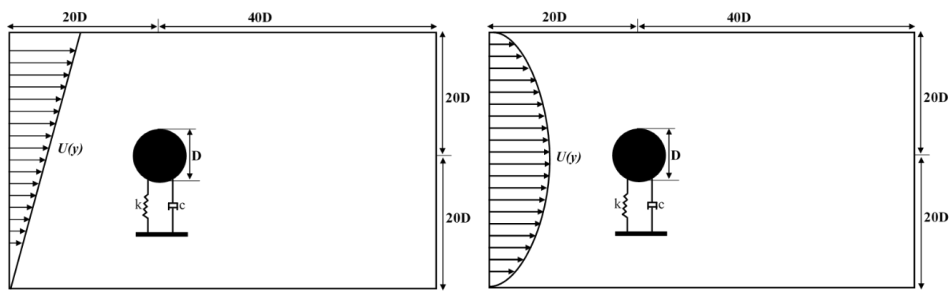

(a) (b)

Figure 1. General system schematic with: (a) linearly shear flow; (b) parabolic flow.

The linearly sheared flow is characterized by the linear velocity profile U(y), which varies with the vertical position y at the inlet:

$$U(y) = U_c + Cy, \qquad (1)$$

where $C = \frac{U_c K}{D}$ is the slope of the velocity profile, where U_c is the centreline velocity and K is the shear parameter. In the current study, low values of K are used with a fixed increment: 0.0, 0.03, 0.05.

The inlet velocity profile for the parabolic flow is defined as:

$$U(y) = U_c\left(1 - \left(\frac{y}{h}\right)^2\right), \qquad (2)$$

where h is the inlet total height of 40D.

The flow around the cylinder is simulated using a transient, incompressible 2D Navier-Stokes equation (Annapeh & Kurushina, 2023)

$$\frac{\partial u}{\partial x} + \frac{\partial v}{\partial y} = 0 \qquad (3)$$

$$\rho\left(\frac{\partial u}{\partial t} + u\frac{\partial u}{\partial x} + v\frac{\partial u}{\partial y}\right) = -\frac{\partial p}{\partial x} + \mu\left(\frac{\partial^2 u}{\partial x^2} + \frac{\partial^2 u}{\partial y^2}\right) \qquad (4)$$

$$\rho\left(\frac{\partial v}{\partial t} + u\frac{\partial v}{\partial x} + v\frac{\partial v}{\partial y}\right) = -\frac{\partial p}{\partial y} + \mu\left(\frac{\partial^2 v}{\partial x^2} + \frac{\partial^2 v}{\partial y^2}\right) \qquad (5)$$

where p is the fluid pressure, u and v are flow velocity components, ρ is the density of the fluid, μ is the dynamic viscosity of the fluid, t is the time, x and y are spatial coordinates.

Simulations are performed with the SIMPLE scheme. The gradient is calculated using the Green Gauss Cell Based method, pressure – using the Second Order scheme and momentum – using the Second Order Upwind scheme.

The elastically mounted cylinder is modelled as a spring-mass system. The cross-flow displacement Y is given by the equation:

$$m\ddot{Y} + 2m\zeta\omega_n\dot{Y} + kY = \frac{1}{2}\rho DU^2 C_L(t), \quad (6)$$

where m represents the mass of the oscillating system, $2m\zeta\omega_n$ is the damping coefficient, ζ is the damping ratio, ω_n is the natural frequency of the cylinder, k is the stiffness coefficient of the spring, $C_L(t)$ is the non-dimensional lift coefficient. The motion of the cylinder is simulated with a User Defined Function UDF. The mesh is set to be dynamic. Smoothing and remeshing technique is applied to all of the cells of the dynamic mesh. The cylinder is assumed stationary at the beginning of the simulation in its initial equilibrium position. The initial conditions for the cross-flow displacement and velocity are $Y(0) = 0$ and $\dot{Y}(0) = 0$.

For the numerical results to be accurate, a mesh independence test is carried for the elastically mounted cylinder under uniform flow for five generated grids. The test is conducted for a Reynolds number of 300, determined for the centreline velocity, corresponding to the flow velocity of 0.03 m/s. The damping ratio of 0 and a time step size of 0.005 are used. The mesh for the computational domain and around the cylinder surface is shown in Figure 2(a) and 2(b). The wake region and the area around the cylinder surface is set to have a higher resolution of mesh density in order to have full detail of the vortex formation. A minimum element size of 0.0003 is used on the cylinder surface. The results for the mesh dependency test are shown in Table 1 with details of the mesh used. The results of current calculations are compared with the numerical results from literature (Zhao & Cheng, 2014), and they agree well. The fourth mesh is selected for further simulations.

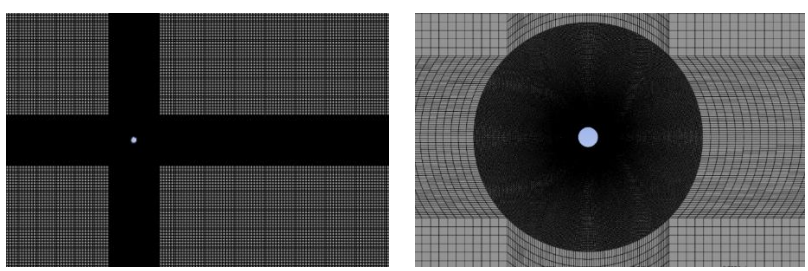

(a) (b)

Figure 2. Computational mesh: (a) mesh for the full domain; (b) zoomed-in mesh around the cylinder

Table 1. Mesh independence test results

Present work	Number of elements	Number of nodes	*Re*	m^*	U_r	Y_{max}/D
Grid 1	58080	29376	300	2	6	0.70
Grid 2	66401	33117				0.65
Grid 3	71807	36260				0.603
Grid 4	84884	42818				0.601
Grid 5	108676	54742				0.593
(Zhao & Cheng, 2014)	-	-	300	2	6	0.60

3. Results and discussion

Numerical simulations are performed in this work for the mass ratio of 2, reduced velocity range of 2-12 and the corresponding Reynolds number range of 350-2200, defined by the centreline velocity. Linearly sheared flow and parabolic flow are considered, and the shear parameter K of the linear flow profile varies between 0 and 0.05. Results are presented below in terms of the maximum displacement amplitude, lift and drag coefficients statistics, frequency ratio and time histories.

Figure 3 shows the maximum displacement amplitude of the cylinder as a function of reduced velocity. Figure 3 shows a steady increase in the displacement for all cases as the reduced velocity grows from 2 to 4, with little difference in between the flows. The maximum displacement amplitude is observed at the reduced velocity of 6 for all considered velocity profiles, and three of the flows demonstrate a similar value of about 0.8D. This result is consistent with the works (Singh & Chatterjee, 2014; Tu et al., 2015). A relatively lower maximum amplitude at this reduced velocity is experienced at the shear parameter of 0.05, together with a wider upper branch. The broadening of the synchronization region, as K increases, shows a reasonable agreement with the work of (Tu et al., 2014). After the peak at $U_r = 6$, there is a decrease in displacement for all flow conditions, especially for the uniform flow at K = 0.0. The drop in displacement is more gradual for shear parameters of K=0.03 and K=0.05 and parabolic flow, and the lower branch in these cases is relatively higher than overall for the uniform flow. The highest displacements are observed in the region of the reduced velocity from 10 to 12 for K = 0.03.

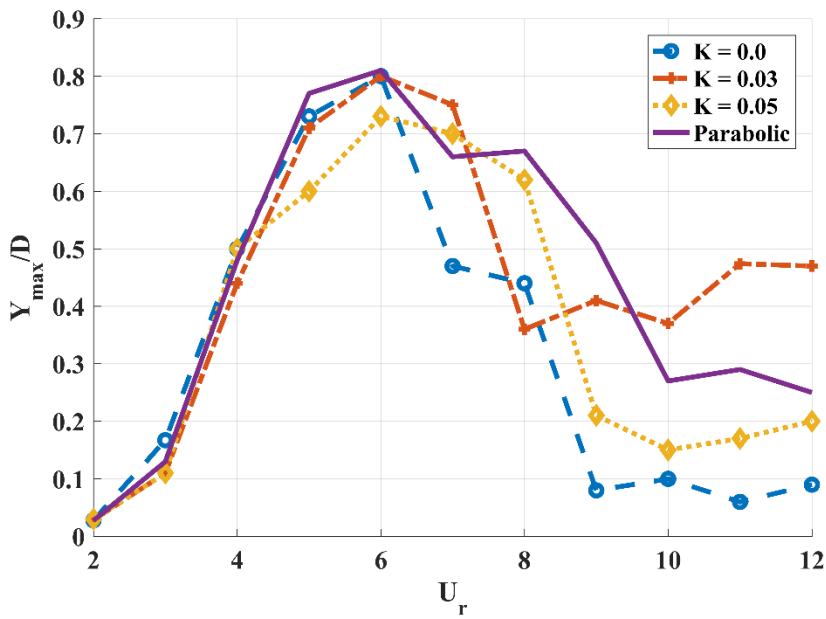

Figure 3. Maximum displacement amplitude vs. reduced velocity

Figure 4 displays the mean drag coefficient acting on the circular cylinder as a function of the reduced velocity for the four flow conditions. The mean drag coefficient generally increases with the reduced velocity for all cases. There are noticeable differences between the flow cases as the reduced velocity increases, particularly beyond Ur =

7. For the reduced velocity of 2-7, there appear to be no significant difference in the mean drag coefficient for all flow conditions. A sharp drop in the mean drag coefficient is observed for the uniform flow of K = 0.0 at the reduced velocity of 8, after which there is a steep rise around U_r =10, reaching the highest $C_{D,mean}$ value of 0.452 by U_r = 12. Shear flows of K=0.03 and K=0.05 both have a steadily increasing mean drag coefficient, and these values are below the uniform flow case at U_r = 12. Overall, the differences in the mean drag coefficient in terms of K are not very significant, and this agrees well with the work (Kang, 2006) for the stationary cylinder in the planar sheared flow. The parabolic flow leads to the lower mean drag coefficient values at the reduced velocities from 9 to 11.

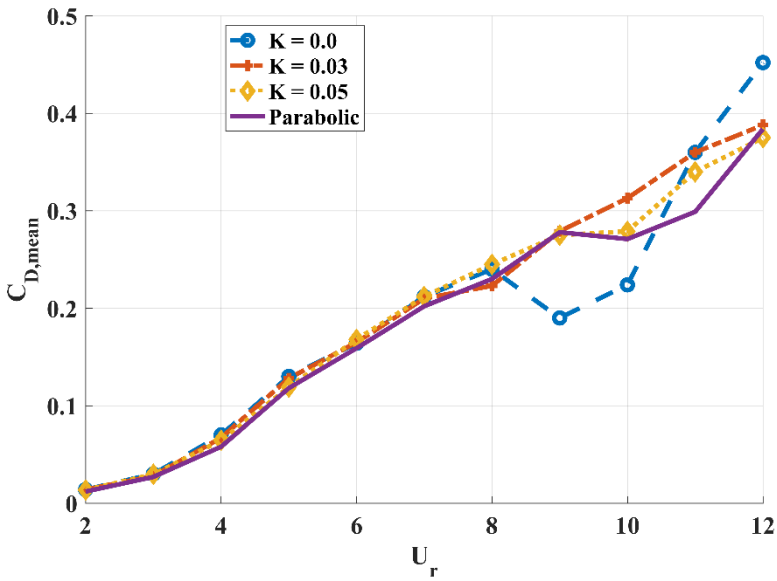

Figure 4. Mean drag coefficient vs. reduced velocity

Figure 5 shows the root mean square (RMS) value of the lift coefficient as a function of the Reynolds number. For all flow conditions, generally, the lift coefficient increases as the Reynolds number rises. Notably, the uniform flow case (K = 0.0) shows a significant spike of the RMS lift coefficient of 0.32 at Re = 2000, while the linearly sheared and parabolic flows exhibit a more gradual increase. A lesser peak is observed at around Re = 900 and 1100 for all flow conditions, which is consistent with the transition from the initial branch to the upper branch. For Re = 350-1000, across all flow cases, the RMS lift coefficient remains below 0.05. As the Reynolds number increases to 1000-1600, the flow cases start to display a different behavior, with sheared flow conditions linked to slightly higher lift fluctuations than the uniform flow. At higher Reynolds numbers of 1600-2200, there appear to be a more distinct behavior between the flow conditions. For the sheared flow cases of K = 0.03 and K = 0.05, the RMS lift coefficient values increase but at a much slower rate, compared to the uniform flow, with a peak value of 0.152 for K = 0.03 at the end of the considered range at Re = 2150. Similar to the linearly sheared flow cases, the lift coefficient in the parabolic flow demonstrates the gradual increase, with the RMS value reaching 0.15 at Re=2150.

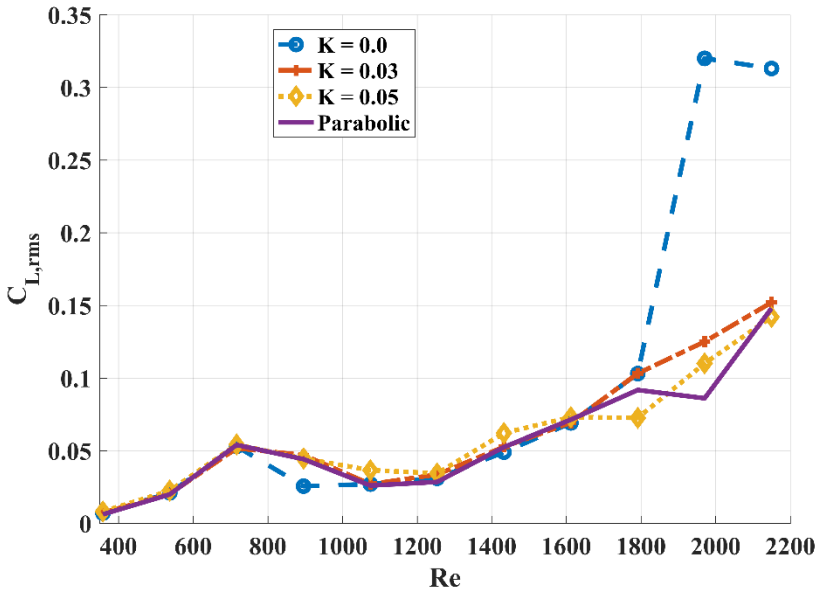

Figure 5. RMS of the lift coefficient vs. Reynolds number

Figure 6 shows the frequency ratio as a function of the reduced velocity for the four flow conditions. The frequency ratio gradually increases as the reduced velocity grows. It appears that the frequency ratio in the parabolic flow is quite close in values to the one in the linearly sheared flow at K = 0.05 for the full range of considered reduced velocities. At the same time, the frequency ratio in the uniform flow conditions is relatively close to the one in the linearly sheared flow at K = 0.03, up until U_r = 8. There is a noticeable rise in the frequency ratio for the K = 0.0 (uniform flow) case, starting past U_r = 8, while the other flow conditions (shear and parabolic) exhibit a much smoother and slower increase. For U_r = 2-5, the frequency ratio starts at around 0.5 for all flow cases and gradually increases to about 0.75. At U_r = 5-7, the frequency ratio is approaching 1.0 for all flow conditions, so that the vibration frequency is close to the natural frequency of the structure.

Figure 7 illustrates the time history of displacement at the reduced velocity of 2 depicting the dynamics during the initial branch of the lock-in peak, displayed in Fig. 3. At this reduced velocity, the displacement and lift coefficient amplitudes for the four flow conditions are relatively small, the signals are stable and in phase with each other. Similar observation is made in the work (Postnikov et al., 2017) for the uniform flow conditions. The lift coefficient in dynamics at this reduced velocity is shown in Appendix A, Figure A1. The FFT for the displacement and lift coefficient time history at this reduced velocity are given in Appendix B in Figure B1 and in Appendix C in Figure C1 respectfully. Here, Figure B1 demonstrates a second relatively prominent frequency peak visible in the FFT spectrum for the displacement signal in the linearly sheared flow at K = 0.05. This second peak is less pronounced or non-existent in other flow conditions. Also, the dominant frequency in the case of the sheared flow with K = 0.05 is relatively lower than in other cases. Figure C1 confirms a single dominant frequency for the lift force signal, with no significant difference in the dominant frequency.

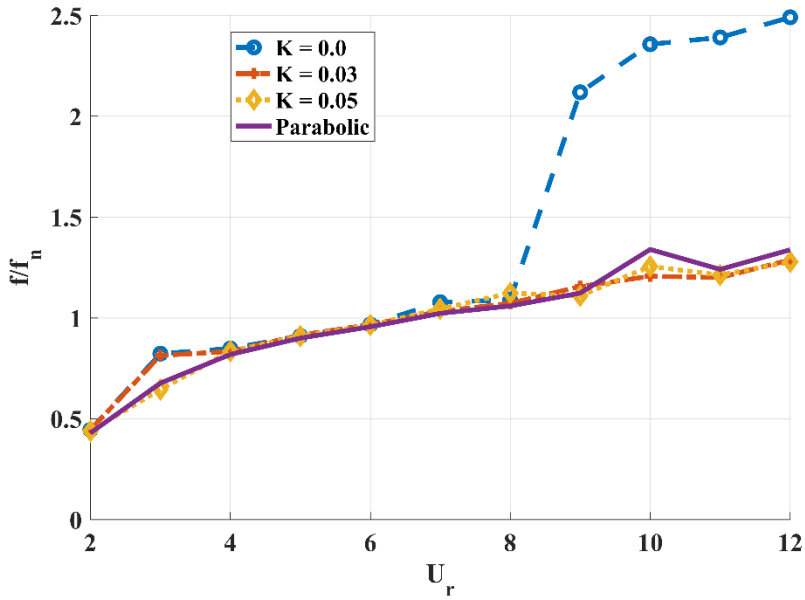

Figure 6. Vibration frequency ratio vs. reduced velocity

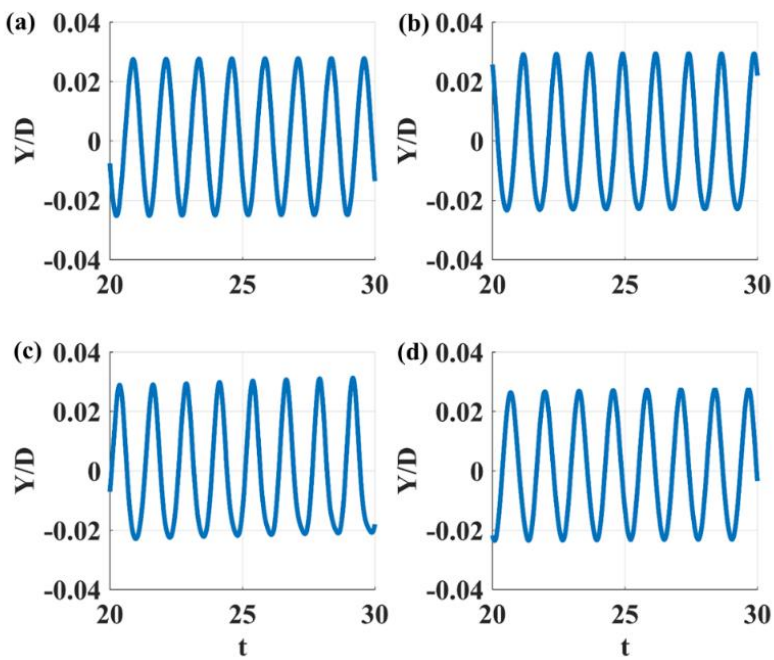

Figure 7. Displacement time history for different flow conditions at the reduced velocity of 2: (a) uniform flow of K = 0.0; (b) linearly sheared flow of K = 0.03; (c) linearly sheared flow of K = 0.05; (d) parabolic flow

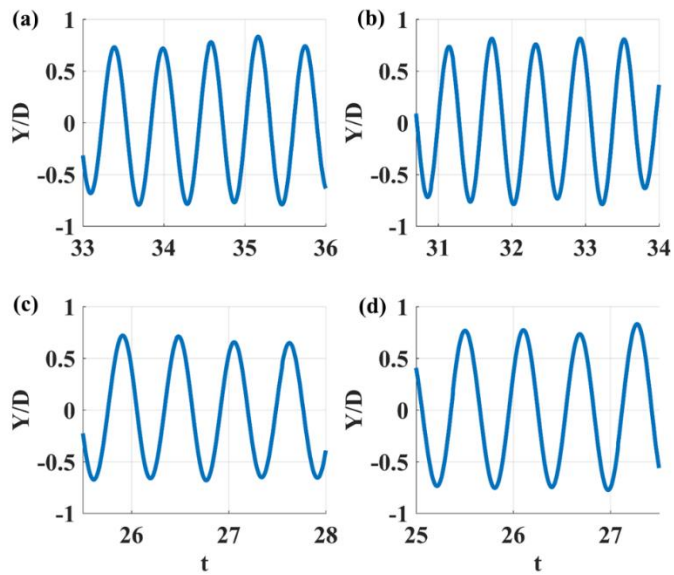

Figure 8. Displacement time history for different flow conditions at the reduced velocity of 6: (a) uniform flow of K = 0.0; (b) linearly sheared flow of K = 0.03; (c) linearly sheared flow of K = 0.05; (d) parabolic flow

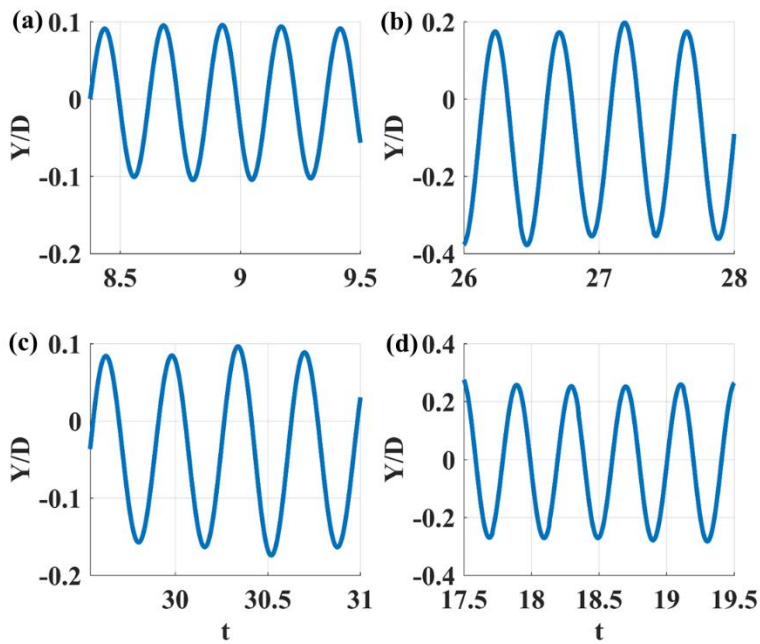

Figure 9. Displacement time history for different flow conditions at the reduced velocity of 10: (a) uniform flow of K = 0.0; (b) linearly sheared flow of K = 0.03; (c) linearly sheared flow of K = 0.05; (d) parabolic flow

Figure 8 shows the displacement of the cylinder as a function of time at the reduced velocity of 6 where the maximum displacement of the cylinder is observed during the upper branch in Figure 3. The corresponding lift coefficient time history is shown in Figure A2 in Appendix A. At this reduced velocity, the displacement and the lift coefficient signals are out of phase and exhibit complex dynamics. The frequency spectrum of the displacement signal in Figure B2 in Appendix B indicates yet a single dominant peak for the uniform and linearly sheared flow conditions at K = 0.03. At the same time, competing frequency peaks are observed for the linearly sheared flow of K = 0.05 and parabolic flow. Also, the dominant oscillation frequency at K = 0.05 appears to be significantly lower than in other cases. Similar effects of the flow conditions are seen for the frequency of the lift coefficient in Figure C2 in Appendix C: with two strong frequencies in the linearly sheared flow of K = 0.05 and parabolic flow, while a single peak manifests in other flow conditions.

Displacement time history at the reduced velocity of 10, corresponding to the lower branch, is shown in Figure 9. Amplitude of the displacement at this reduced velocity is significantly lower compared to the upper branch. The displacement signal in Figure 9 and the lift coefficient in Figure A3 in Appendix A are out of phase. Also, some asymmetry is present in the displacement signals in the linearly sheared flow in Figure 9(b) and 9(c). The frequency spectra in Figure B3 and C3 in Appendix B and C respectively indicate overall lower dominant frequencies in sheared flow, compared to the uniform flow, for both dynamics of the displacement and the lift coefficient. At the reduced velocity of 10, several competing peaks are present in all PSD diagrams, with particularly strong competition of peaks in the parabolic flow conditions and in the linearly sheared flow of K = 0.05.

4. Conclusion

The present study investigates the dynamic behavior of an elastically mounted circular cylinder oscillating in the transverse direction subjected to planar sheared flow of varying shear parameter (K= 0.0, 0.03 and 0.05) and parabolic flow using the computational fluid dynamics approach. The simulations are conducted for the mass ratio of 2 and a damping ratio of 0. It is found that the maximum displacement value of 0.81 at a reduced velocity of 6 is observed for the uniform and parabolic flow in the upper branch. The linearly sheared flow conditions at K = 0.03 lead to the highest displacement in the lower branch.

Also, it is shown in the results, that the mean drag coefficient increases significantly for the uniform flow case, as the reduced velocity increases past Ur = 10. It is found, that the shear flow cases and the parabolic flow exhibit a more stable mean drag coefficient across the entire range of reduced velocities.

In the uniform flow case (K = 0.0), the root mean square (rms) of the lift coefficient (CLrms) shows a sharp increase at higher reduced velocities, particularly beyond Ur = 10. For the shear flow cases (K=0.0 and K=0.05) and parabolic flow, the CLrms remains relatively low and stable across the reduced velocity range. The gradual increase in CLrms suggests that shear flow disrupts the formation of large, coherent vortices that would otherwise contribute to strong lift oscillations.

Analysis also indicates reduction in the vibration frequency in the sheared flow compared to the uniform flow during the lower branch. Multiple frequencies are found in the signals of displacement and lift coefficient during the upper and lower branches leading to the complex dynamics, which is particularly relevant to the linearly sheared flow at K = 0.05 and parabolic flow profiles.

Overall, effects of the linearly sheared and parabolic flows appear to lead to a stable pattern in the mean drag coefficient, partially reduced lift coefficient, lower vibration frequencies, however, also to more complex displacement and force fluctuations. Effect of the specific dominant flow profile should be taken into account during the design stage of offshore structures.

Acknowledgment: The authors would like to acknowledge the support of the National Project "Science and Universities" of the Ministry of Science and Higher Education of the Russian Federation, grant number FEWN-2024-0005

References:

Akosile, O. O., & Sumner, D. (2003). Staggered circular cylinders immersed in a uniform planar shear flow. *Journal of Fluids and Structures, 18*(5), 613–633.

Annapeh, H. F., & Kurushina, V. (2022). Analysis of vortex-induced forces on the group of subsea structures in proximity of equipment at Re = 3900. *Journal of Mathematical Structures and Modelling, 4*(64), 60–74.

Annapeh, H. F., & Kurushina, V. (2023). Flow-induced forces for a group of one large and several small structures in the sheared turbulent flow. *Fluids, 8*(5), Article 158. https://doi.org/10.3390/fluids8050158

Annapeh, H. F., & Kurushina, V. (2024). Linear sheared flow effects in vortex-induced forces on three tandem subsea structures in proximity to larger objects. In W. Lacarbonara (Ed.), *Advances in nonlinear dynamics, Volume I. ICNDA 2023* (NODYCON Conference Proceedings Series). Springer. https://doi.org/10.1007/978-3-031-50631-4_2

Bearman, P. W. (1984). Vortex shedding from oscillating bluff bodies. *Annual Review of Fluid Mechanics, 16*, 195–222.

Bhattacharyya, S., & Dhinakaran, S. (2008). Vortex shedding in shear flow past tandem square cylinders in the vicinity of a plane wall. *Journal of Fluids and Structures, 24*(3), 400–417.

Blevins, R. (1990). *Flow-induced vibration*. Van Nostrand Reinhold.

Blevins, R. D., & Coughran, C. S. (2009). Experimental investigation of vortex-induced vibration in one and two dimensions with variable mass, damping, and Reynolds number. *Journal of Fluids Engineering, 131*(10). https://doi.org/10.1115/1.3222904

Cao, S., Ge, Y., & Tamura, Y. (2012). Shear effects on flow past a square cylinder at moderate Reynolds numbers. *Journal of Engineering Mechanics, 138*(1), 116–123.

Cheng, M., Tan, S. H. N., & Hung, K. C. (2005). Linear shear flow over a square cylinder at low Reynolds number. *Physics of Fluids, 17*(7), Article 078103. https://doi.org/10.1063/1.1985790

Kang, S. (2006). Uniform-shear flow over a circular cylinder at low Reynolds numbers. *Journal of Fluids and Structures, 22*(4), 541–555.

Khalak, A., & Williamson, C. H. K. (1996). Dynamics of a hydroelastic cylinder with very low mass and damping. *Journal of Fluids and Structures, 10*(5), 455–472.

Khan, N. B., Ibrahim, Z., Nguyen, L. T. T., Javed, M. F., & Jameel, M. (2017). Numerical investigation of the vortex-induced vibration of an elastically mounted circular cylinder at high Reynolds number ($Re=10^4$) and low mass ratio using the RANS code. *PLoS ONE, 12*(10), Article e0185832.

Lankadasu, A., & Vengadesan, S. (2008). Interference effect of two equal-sized square cylinders in tandem arrangement: With planar shear flow. *International Journal for Numerical Methods in Fluids, 57*(8), 1005–1021.

Lu, X., Dalton, C., & Zhang, J. (1997). Application of large eddy simulation to an oscillating flow past a circular cylinder. *Journal of Fluids Engineering, 119*(3), 519–525. https://doi.org/10.1115/1.2819275

Martins, F. A. C., & Avila, J. P. J. (2019). Effects of the Reynolds number and structural damping on vortex-induced vibrations of elastically-mounted rigid cylinder. *International Journal of Mechanical Sciences, 156*, 235–249.

Postnikov, A., Pavlovskaia, E., & Wiercigroch, M. (2017). 2DOF CFD calibrated wake oscillator model to investigate vortex-induced vibrations. *International Journal of Mechanical Sciences, 127*, 176–190. https://doi.org/10.1016/j.ijmecsci.2016.05.019

Sarpkaya, T. (2004). A critical review of the intrinsic nature of vortex-induced vibrations. *Journal of Fluids and Structures, 19*(4), 389–447.

Singh, S. P., & Chatterjee, D. (2014). Impact of transverse shear on vortex induced vibrations of a circular cylinder at low Reynolds numbers. *Computers & Fluids, 93*, 61–73.

Stappenbelt, B., Lalji, F., & Tan, G. (2007). Low mass ratio vortex-induced motion. In *Proceedings of the 16th Australasian Fluid Mechanics Conference* (pp. 1491–1497). University of Queensland. https://espace.library.uq.edu.au/view/UQ:120983

Tu, J., Zhou, D., Bao, Y., Fang, C., Zhang, K., Li, C., & Han, Z. (2014). Flow-induced vibration on a circular cylinder in planar shear flow. *Computers & Fluids, 105*, 138–154.

Tu, J., Zhou, D., Bao, Y., Ma, J., Lu, J., & Han, Z. (2015). Flow-induced vibrations of two circular cylinders in tandem with shear flow at low Reynolds number. *Journal of Fluids and Structures, 59*, 224–251.

Williamson, C. H. K., & Govardhan, R. (2004). Vortex-induced vibrations. *Annual Review of Fluid Mechanics, 36*(1), 413–455.

Williamson, C. H. K., & Roshko, A. (1988). Vortex formation in the wake of an oscillating cylinder. *Journal of Fluids and Structures, 2*(4), 355–381.

Zhang, H., Fan, B. C., Chen, Z. H., Li, H. Z., & Li, B. M. (2014). An in-depth study on vortex-induced vibration of a circular cylinder with shear flow. *Computers & Fluids, 100*, 30–44.

Zhao, M., & Cheng, L. (2014). Vortex-induced vibration of a circular cylinder of finite length. *Physics of Fluids, 26*(1), Article 015111. https://doi.org/10.1063/1.4862548

Zhao, M., Cheng, L., & An, H. (2012). Numerical investigation of vortex-induced vibration of a circular cylinder in transverse direction in oscillatory flow. *Ocean Engineering, 41*, 39–52.

Henry Francis Annapeh
Industrial University of Tyumen
Tyumen,
Russia
annapeg@tyuiu.ru
ORCID 0000-0003-1256-499X

Victoria Kurushina
Industrial University of Tyumen
Tyumen,
Russia
kurushinava@tyuiu.ru
ORCID 0000-0001-9294-5789

Appendix A

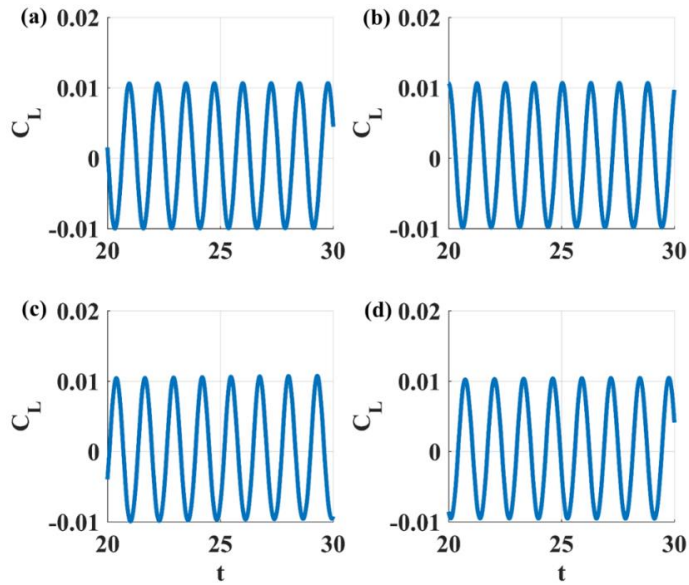

Figure A1. Lift coefficient time history for: (a) K = 0.0, (b) K = 0.03, (c) K = 0.05, (d) Parabolic at reduced velocity of 2

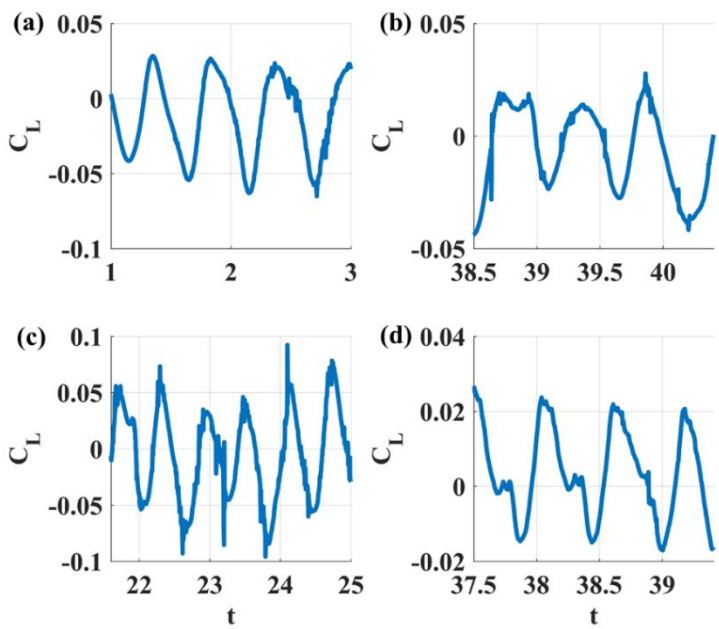

Figure A2. Lift coefficient time history for: (a) K = 0.0, (b) K = 0.03, (c) K = 0.05, (d) Parabolic at reduced velocity of 6

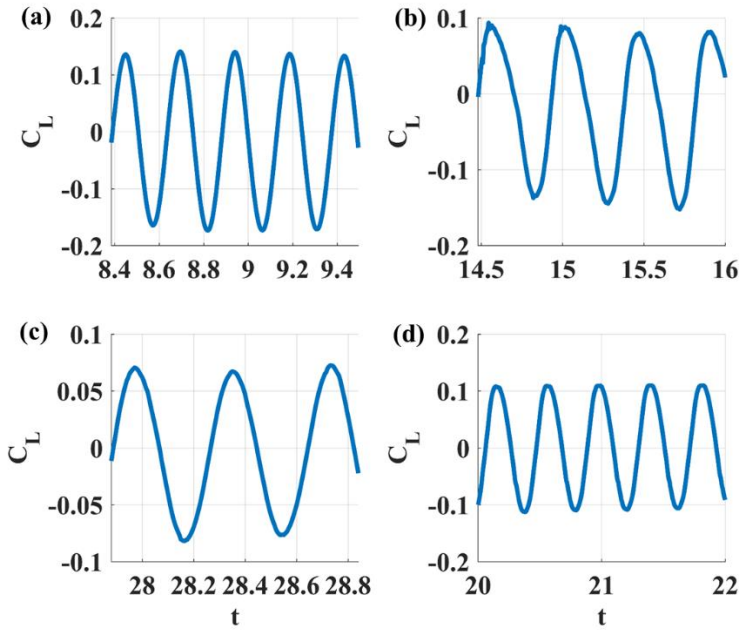

Figure A3. Lift coefficient time history for: (a) K = 0.0, (b) K = 0.03, (c) K = 0.05, (d) Parabolic at reduced velocity of 10

Appendix B

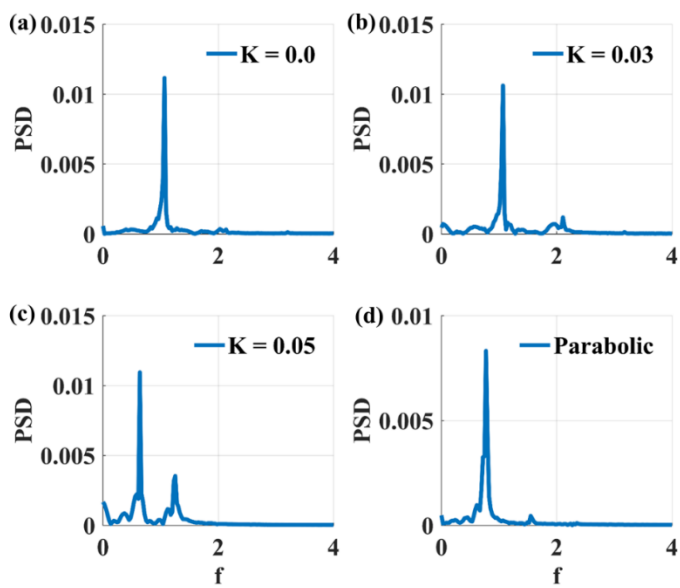

Figure B1. The FFT for displacement time history at (a) K = 0.0, (b) K = 0.03, (c) K = 0.05, (d) Parabolic at reduced velocity of 2

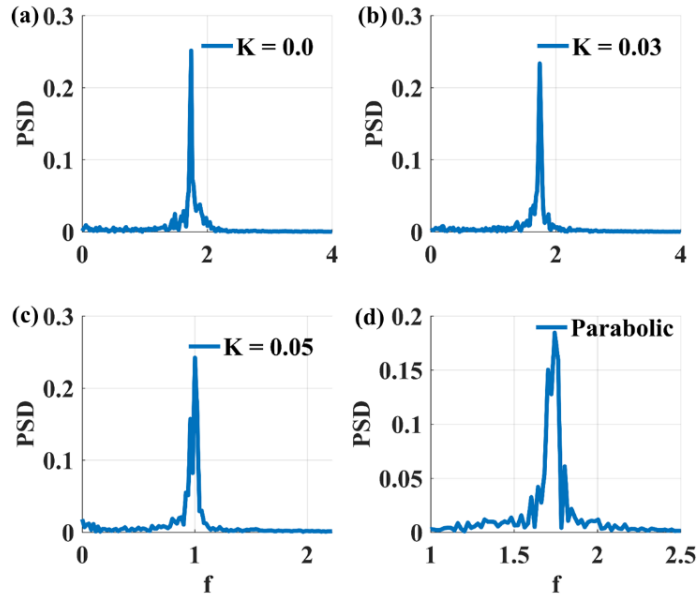

Figure B2. The FFT for displacement time history at (a) K = 0.0, (b) K = 0.03, (c) K = 0.05, (d) Parabolic at reduced velocity of 6

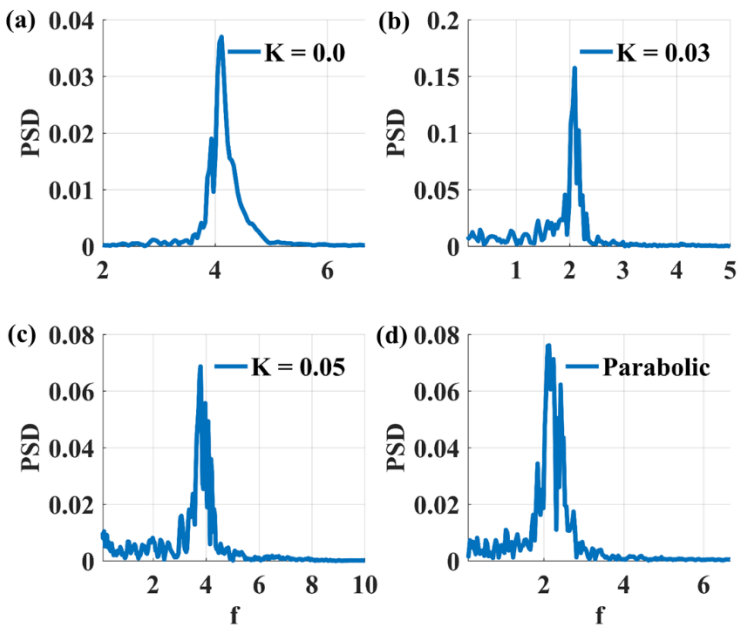

Figure B3. The FFT for displacement time history at (a) K = 0.0, (b) K = 0.03, (c) K = 0.05, (d) Parabolic at reduced velocity of 10

Appendix C

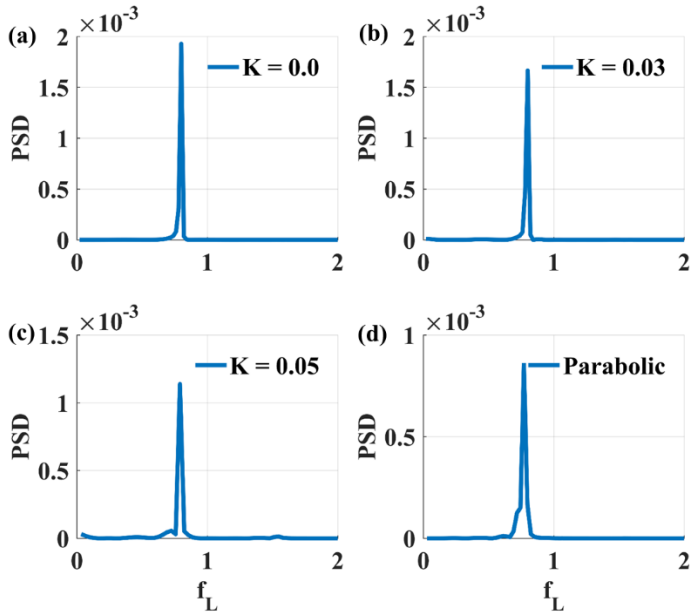

Figure C1. The FFT for lift coefficient time history at (a) K = 0.0, (b) K = 0.03, (c) K = 0.05, (d) Parabolic at reduced velocity of 2

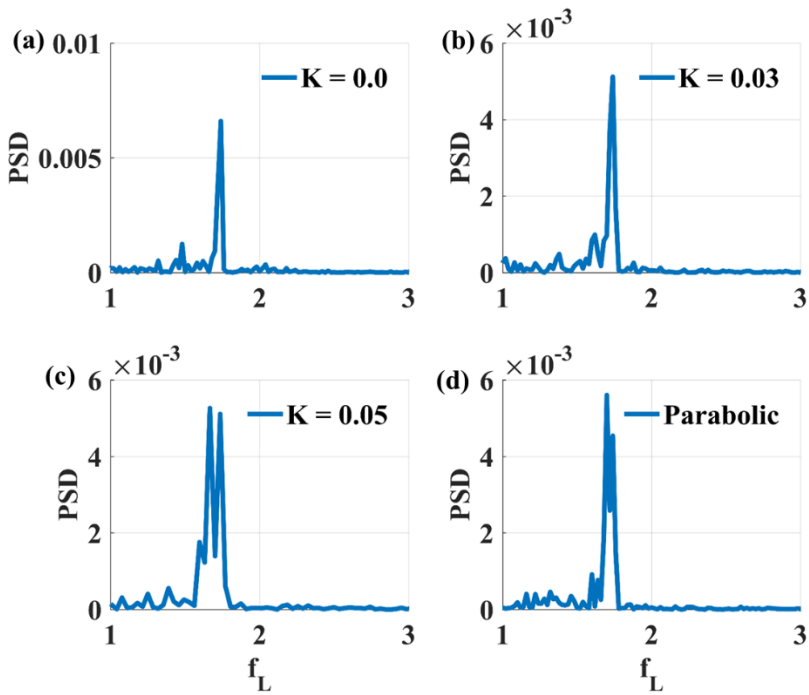

Figure C2. The FFT for lift coefficient time history at (a) K = 0.0, (b) K = 0.03, (c) K = 0.05, (d) Parabolic at reduced velocity of 6

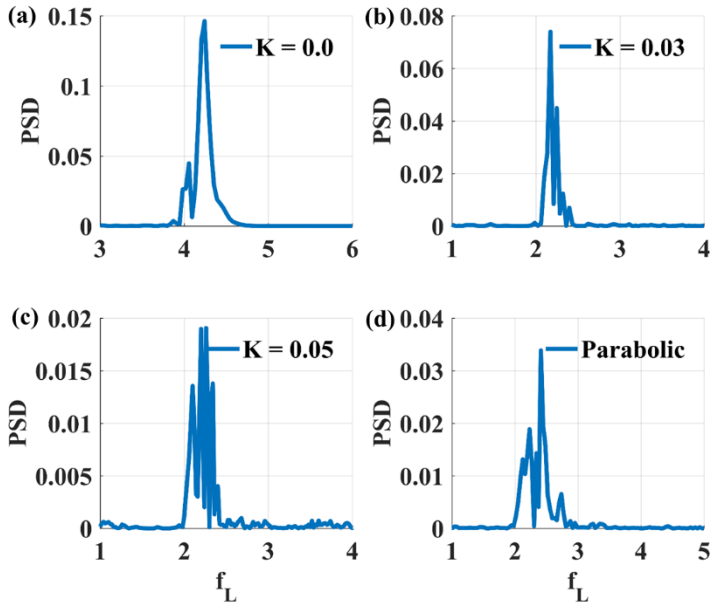

Figure C3. The FFT for lift coefficient time history at (a) K = 0.0, (b) K = 0.03, (c) K = 0.05, (d) Parabolic at reduced velocity of 10